Composite Structures 280 (2022) 114916

Contents lists available at ScienceDirect

Composite Structures

journal homepage: www.elsevier.com/locate/compstruct

Simplified plasticity damage model for large rupture strain (LRS) FRP-confined concrete

Yu-Lei Bai [a], Yu-Feng Zhang [a], Jun-Feng Jia [a,*], Shi-Jie Mei [a], Qiang Han [a], Jian-Guo Dai [b]

[a] Key Laboratory of Urban Security and Disaster Engineering of Ministry of Education, Beijing University of Technology, Beijing, China
[b] Department of Civil and Environmental Engineering, The Hong Kong Polytechnic University, Hong Kong, China

ARTICLE INFO

Keywords:
LRS FRP
RC columns
Simplified plasticity damage model
Cyclic axial compression
Pseudo-plastic strain

ABSTRACT

Large rupture strain (LRS) fiber-reinforced polymers (FRP) composites with an elongation greater than 5% offer an attractive solution for seismic strengthening of reinforced concrete (RC) columns. For a quick and reliable design of LRS FRP-strengthened RC columns, this paper presents a simplified plasticity damage model for LRS FRP-confined concrete under cyclic axial compression. This model consists of two parts: (a) a recent monotonic LRS FRP-confined concrete model developed by the authors' group as an envelope curve and (b) a simplified linear plasticity damage cyclic rule for predicting unloading and reloading paths. To solve the cyclic model deviation induced by concrete softening under a large axial strain, a pseudo-plastic strain was proposed, based on which the damage degradation of FRP-confined concrete can be quantified. The model comparisons show that although the proposed model sacrificed some precision when directly applied for the cyclic axial compressive behavior of FRP-confined concrete, it can give similarly accurate predictions as a complex model does for the behavior of conventional or LRS FRP-jacketed RC columns under a combined axial load and cyclic lateral load. Thus, this simplified plasticity damage model serves as a promising basic model for simulation of the seismic performance of FRP-strengthened structures.

1. Introduction

It is well-known that fiber-reinforced polymer (FRP) composites have the characteristics of light weight, high strength and anti-corrosion. Furthermore, FRP confinement can effectively improve the strength and ductility of concrete. As a result, FRP has been widely used in the seismic retrofitting and strengthening of reinforced concrete (RC) structures for the past three decades [1-15]. The commonly used FRP materials (e.g., CFRP and GFRP) are usually referred as conventional FRPs [16,17]. These FRPs exhibit a high elastic modulus and a linear tensile stress–strain relationship with a small tensile rupture strain ranging from 1.5% to 3%. In recent years, newly-developed large rupture strain (LRS) FRP composites with a rupture strain of more than 5% have attracted extensive attention. LRS FRPs are manufactured from polyethylene naphthalate (PEN) and polyethylene terephthalate (PET) fibers which are more environmentally friendly as they can be made from waste plastics. In contrast to conventional FRPs, LRS FRPs possess an approximately bilinear stress–strain relationship and a higher rupture strain (Fig. 1). Existing studies have shown that LRS FRP-confined concrete can exhibit superior ductility and energy absorption behavior, providing a favorable alternative seismic strengthening solution for structural components when ductility enhancement is of primary significance [16-30]. To further explore the advantage of its large rupture strain characteristic, recently, the authors' group has also paid attention to the impact behavior of LRS FRP-strengthened RC structures [31-34].

Accurate modeling of the cyclic axial behavior of LRS FRP-confined concrete is the basis for seismic analysis of LRS FRP-wrapped RC columns. However, most cyclic FRP-confined concrete models were developed for conventional FRP-wrapped specimens [4,6,8,9,11-14]. It is evident that the properties of LRS FRPs are distinct from those of conventional FRPs. Since the confined concrete's cyclic behavior is largely reliant on the physical properties of confining materials, the direct extension of conventional FRP-confined concrete models to concrete wrapped with LRS FRP without proper modification may result in an inappropriate design. Dai et al. [19] conducted compressive tests on concrete cylinders wrapped with PEN and PET FRP composites and compared the test results with the predictions of Jiang and Teng model

* Corresponding author.
E-mail addresses: baiyulei@bjut.edu.cn (Y.-L. Bai), yfzbjut@163.com (Y.-F. Zhang), jiajunfeng@bjut.edu.cn (J.-F. Jia), meisj2020@163.com (S.-J. Mei), qhan@bjut.edu.cn (Q. Han), cejgdai@polyu.edu.hk (J.-G. Dai).

https://doi.org/10.1016/j.compstruct.2021.114916
Received 14 September 2021; Received in revised form 22 October 2021; Accepted 28 October 2021
Available online 3 November 2021
0263-8223/

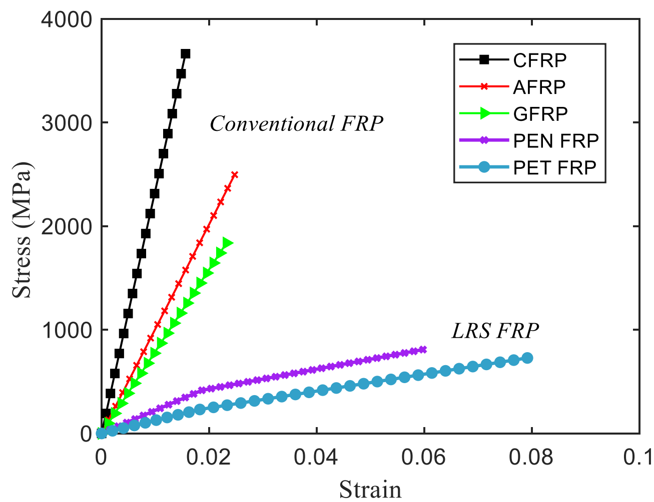

Fig. 1. Typical tensile stress–strain curves of conventional FRP and LRS FRP.

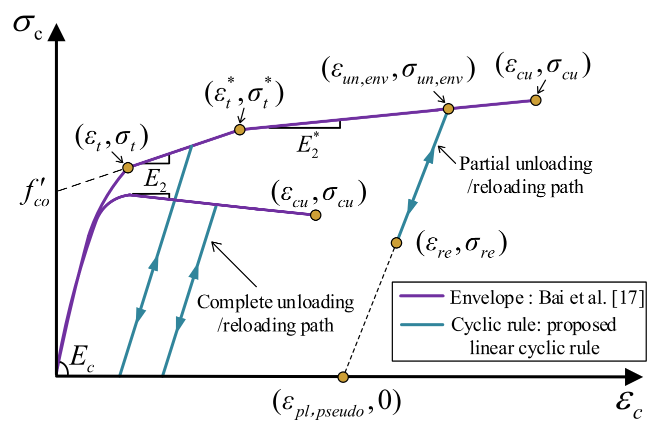

Fig. 2. Simplified plasticity damage model for LRS FRP-confined concrete.

[7]. They discovered that the model could not accurately estimate the ultimate axial strain of LRS FRP-wrapped columns and thus developed a revised version. Ispir [24] carried out an experiment of PET FRP-wrapped cylinders subjected to monotonic and cyclic axial compression and evaluated some existing models using with experimental data. The evaluations also showed that models for conventional FRP-confined concrete are incapable of making reliable predictions. Bai et al. [17] examined many circular LRS FRP-confined columns and established a vast test database for conventional and LRS FRP-wrapped circular specimens. They found that most models for conventional FRP-confined concrete might lead to significant deviation of the final condition when the axial strain becomes larger; hence, Bai et al. [17] developed an axial compressive model for LRS FRP-confined circular specimens. Pimanmas and Saleem [29] evaluated a series of steel and FRP-confined concrete models to forecast the ultimate conditions of PET FRP-confined concrete. They found that very few models could accurately predict the ultimate stress and strain of PET FRP-confined concrete. However, for a quick and reliable design of RC columns requiring seismic retrofitting with LRS FRP, the cyclic axial response of LRS FRP-confined concrete needs to be precisely modeled [35].

Currently, the authors' group performed the first investigation into the responses of LRS FRP-wrapped columns under cyclic axial compression and developed a cyclic stress–strain model [22]. However, this model is in essence an analysis-oriented model that predicts the envelope stress–strain response via an incremental process. In comparison to the analysis-oriented model, a design-oriented model can directly give more straightforward predictions, which facilitates an easier engineering application. Recently, by combining a stiffness-based envelope model [17] and the widely used cyclic rule framework in Lam and Teng model [8], the authors' group further developed a cyclic design-oriented model [36]. This novel model had proved capable of making accurate predictions for the response of LRS FRP-confined concrete; however, the model is still very complicated with cumbersome formulas for the cyclic rule, which may hinder its practical applications in seismic design. On the other hand, the classical cyclic stress–strain models for concrete (Karsan and Jirsa [37] and Lee et al.[38]) widely adopted a simplified linear cyclic rule for the cyclic unloading and reloading loops. This simplification has been adopted by several concrete models in OpenSees [39] and ABAQUS [40] platforms, which was proved to be reliable and effective. Clearly, this straight-line form is much easier to be used than the existing curved one for FRP-confined concrete.

Against this background, this paper presents the first-ever simplified plasticity damage model for LRS FRP-confined concrete subjected to cyclic axial compression. The cyclic criterion of the proposed model was developed based on a linear cyclic rule that can simplify the unloading and reloading paths. The above mentioned monotonic model of Bai et al. [17] was adopted as the envelope of the proposed simplified model. Fig. 2 presents a schematic representation of the simplified plasticity damage model. The supporting calculations addressing the various stresses and strains imposed by the FRP confinement shown in this figure are discussed in Section 3. The performance of the developed model was first assessed by comparing its predictions with cyclic axial compression test results. Subsequently, the proposed model was implemented as a new uniaxial material model in OpenSees [39] platform and the seismic performance of conventional and LRS FRP-strengthened RC piers was evaluated through numerical analysis. Results indicated that the proposed model is inferior to the existing model with unloading and reloading rules of sophisticated forms in forecasting the cyclic axial response of an FRP-confined concrete cylinder. However, the proposed model can provide acceptably accurate predictions of the behaviors of conventional and LRS FRP-jacketed RC columns under a combined axial and cyclic lateral load while avoiding the complexity of the previous models. Therefore, this simplified plasticity damage model serves as a promising basic model for seismic simulation of FRP-strengthened concrete structures.

2. Test database

Although this paper mainly focuses on the cyclic axial model of LRS FRP-confined concrete, the target model is also expected to be applicable to conventional FRP-confined concrete. Thus, an experimental database comprised of both conventional and LRS FRP-wrapped circular concrete columns was established based on the existing research of Lam et al. [5], Wang et al. [10], Li et al. [13], Bai et al. [22], and Ispir [24]. The unconfined concrete strength from standard plain concrete cylinders varies from 24.1 to 60.5 MPa. Detailed information is summarized in Tables 1 and 2. The database includes both stress-hardening and stress-softening curves. At each specified unloading displacement/load level, most columns were exposed to one unloading/reloading cycle. Two columns (CI-RC and CII-RC) from Lam et al. [5] and eight columns from Bai et al. [22] were exposed to multiple internal cycles at each specified envelope's unloading displacement/load level. For more detailed information, readers can refer to the original papers.

3. Simplified plasticity damage model for LRS FRP-confined concrete

3.1. Monotonic stress–strain model for the envelope curve

Traditionally, the envelope curve of an FRP-confined concrete column under an axial cyclic load was believed to be the same as that of axial compressive responses of the same column under a monotonic load

Table 1
Database: cyclic compression tests of conventional FRP-confined concrete.

	Refs.	Specimen	D/h (mm)	f_{co}' (MPa)	FRP ply no.	t_{frp} (mm)	E_{frp} (GPa)	$\varepsilon_{h,rup}$	ε_{cu}	f_{cu}' (MPa)
1	Lam et al. [5]	CI-SC1	152/305	41.1	1	0.165	250	0.0132	0.0134	60.2
2		CI-SC2		41.1	1	0.165	250	0.0103	0.0117	56.8
3		CI-RC		41.1	1	0.165	250	0.0113	0.0120	56.5
4		CII-SC1		38.9	2	0.330	247	0.0122	0.0244	81.5
5		CII-SC2		38.9	2	0.330	247	0.0108	0.0189	78.2
6		CII-RC		38.9	2	0.330	247	0.0122	0.0234	85.6
7	Wang et al. [10]	C2H0L1C	204/612	24.5	1	0.165	244	0.0147	0.0194	42.3
8		C2H0L2C		24.5	2	0.330	244	0.0136	0.0382	46.5
9	Li et al. [13]	C25P0.3C1	150/300	25.0	0.3	0.050	242	0.0182	0.0110	28.4
10		C25P0.3C2		25.0	0.3	0.050	242	0.0171	0.0080	28.8
11		C25P1C1		25.0	1	0.167	242	0.0172	0.0280	54
12		C25P1C2		25.0	1	0.167	242	0.0194	0.0290	56.4
13		C35P0.3C1		35.0	0.3	0.050	242	0.0180	0.0100	40.9
14		C35P0.3C2		35.0	0.3	0.050	242	0.0182	0.0099	41.2
15		C35P1C1		35.0	1	0.167	242	0.0217	0.0232	71.7
16		C35P1C2		35.0	1	0.167	242	0.0183	0.0232	73.4
17		C50P0.3C1		50.0	0.3	0.050	242	0.0194	0.0080	30.1
18		C50P0.3C2		50.0	0.3	0.050	242	0.0173	0.0079	35.0
19		C50P0.5C1		50.0	0.5	0.084	242	0.0162	0.0099	54.2
20		C50P0.5C2		50.0	0.5	0.084	242	0.0192	0.0087	52.9
21		C50P0.75C1		50.0	0.75	0.125	242	0.0169	0.0123	60.4
22		C50P0.75C2		50.0	0.75	0.125	242	0.0172	0.0135	60.1
23		C50P1C1		50.0	1	0.167	242	0.0178	0.0157	69.4
24		C50P1C2		50.0	1	0.167	242	0.0214	0.0162	72.0
25		C60P0.3C1		60	0.3	0.050	242	0.0172	0.0060	53.2
26		C60P0.3C2		60	0.3	0.050	242	0.0190	0.0050	49.1
27		C60P1C1		60	1	0.167	242	0.0210	0.0104	71.6
28		C60P1C2		60	1	0.167	242	0.221	0.0104	71.9

Table 2
Database: cyclic compression tests of LRS FRP-confined concrete.

No.	Refs.	Specimen	D/h (mm)	f_{co}' (MPa)	FRP ply no.	t_{frp} (mm)	E_{frp1} (GPa)	E_{frp2} (GPa)	$\varepsilon_{h,rup}$	ε_{cu}	f_{cu}' (MPa)
1	Bai et al. [22]	PEN-b1-1-A	152/305	35.6	1	1.272	27.0	12.0	0.0480	0.0437	61.2
2		PEN-b1-1-B		35.6	1	1.272	27.0	12.0	0.0516	0.0550	70.2
3		PEN-b1-2-A		35.6	2	2.544	27.0	12.0	0.0558	0.0752	102.1
4		PEN-b1-2-C		35.6	2	2.544	27.0	12.0	0.0568	0.0796	107.3
5		PET-b1-1-A		35.6	1	0.841	17.9	8.3	0.0614	0.0486	47.2
6		PET-b1-1-C		35.6	1	0.841	17.9	8.3	0.0653	0.0624	50.3
7		PET-b1-2-A		35.6	2	1.682	17.9	8.3	0.0796	0.0798	70.1
8		PET-b1-2-C		35.6	2	1.682	17.9	8.3	0.0858	0.0804	77.0
9		PEN-b2-1-A		46.2	1	1.272	27.0	27.0	0.0432	0.0356	63.5
10		PEN-b2-1-B		46.2	1	1.272	27.0	27.0	0.0545	0.0443	69.4
11		PEN-b2-2-A		46.2	2	2.544	27.0	27.0	0.0535	0.0700	112.3
12		PEN-b2-2-B		46.2	2	2.544	27.0	27.0	0.0436	0.0697	107.9
13		PET-b2-2-A		46.2	2	1.682	17.9	8.3	0.0650	0.0660	77.2
14		PET-b2-2-B		46.2	2	1.682	17.9	8.3	0.0684	0.0730	68.1
15		PET-b2-3-A		46.2	3	2.532	17.9	8.3	0.0594	0.0749	94.9
16		PET-b2-3-C		46.2	3	2.532	17.9	8.3	0.0734	0.0853	106.8
17	Ispir [24]	1P-C-a	150/300	24.1	1	1.262	17.9	8.3	0.054	0.0510	47.2
18		1P-C-b		24.1	1	1.262	17.9	8.3	0.053	0.0570	44.0
19		2P-C-a		24.1	2	2.524	17.9	8.3	0.084	0.1030	88.6
20		2P-C-b		24.1	2	2.524	17.9	8.3	–	0.0930	75.4

[6,8-10,36]. This study introduces a monotonic stress–strain model developed by the authors' group [17], which is employed here to forecast the envelope of the proposed simplified model (Fig. 2). This model consists of a parabolic first segment plus a linear second segment with a smooth transition at ε_t, and a linear third segment intersects the linear second segment at ε_t*. The FRP-confined concrete's axial compressive stress and strain relationships are expressed as follows:

$$\sigma_c = \begin{cases} E_c\varepsilon_c - \dfrac{(E_c - E_2)^2}{4f_{co}^{'}}\varepsilon_c^2, 0\leqslant\varepsilon_c\leqslant\varepsilon_t \\ f_{co}^{'} + E_2\varepsilon_c, \varepsilon_t\leqslant\varepsilon_c\leqslant\varepsilon_t^* \\ \sigma_t^* + E_2^*\left(\varepsilon_c - \varepsilon_t^*\right), \varepsilon_t^*\leqslant\varepsilon_c\leqslant\varepsilon_{cu} \end{cases} \quad for\, E_2 \geqslant 0 \tag{1}$$

and

$$\sigma_c = \begin{cases} E_c\varepsilon_c - \dfrac{E_c^2}{4f_{co}^{'}}\varepsilon_c^2, 0\leqslant\varepsilon_c\leqslant\varepsilon_t \\ \sigma_t + E_2(\varepsilon_c - \varepsilon_t), \varepsilon_t\leqslant\varepsilon_c\leqslant\varepsilon_t^* \\ \sigma_t^* + E_2^*\left(\varepsilon_c - \varepsilon_t^*\right), \varepsilon_t^*\leqslant\varepsilon_c\leqslant\varepsilon_{cu} \end{cases} \quad for\, E_2 < 0 \tag{2}$$

where σ_c and ε_c are axial compressive stress and strain of FRP-confined concrete, respectively; f_{co}' is the peak axial stress of unconfined concrete; E_c is the elastic modulus of unconfined concrete determined based on American Concrete Institute (ACI) equation ($E_c = 4700\sqrt{f_{co}'}$) [41]; σ_t and σ_t* are the stress at ε_t and ε_t*, respectively. The slopes of the linear second and third portions, E_2 and E_2*, are given by:

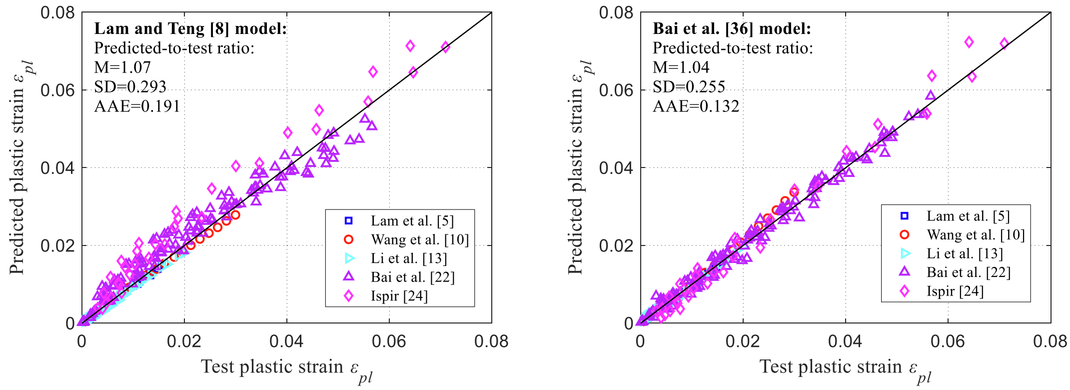

(a) Lam and Teng [8] model (b) Bai et al. [36] model

Fig. 3. Performance of plasticity strain models for envelope cycles.

$$\frac{E_2}{f'_{co}} = -259.8\rho^{-0.5} + 108.5 \tag{3}$$

$$\frac{E_2^*}{f'_{co}} = -57.7(\rho^*)^{-0.5} + 38.1 \tag{4}$$

where ρ (ρ^*) is the confinement rigidity defined by:

$$\rho = \frac{2E_{frp}t_{frp}}{Df'_{co}} \tag{5}$$

Because the LRS FRP has a bilinear stress–strain relationship, two elastic moduli, E_{frp1} and E_{frp2}, of LRS FRP are incorporated into the above calculation to obtain $\rho$and ρ^*, respectively. In Eqs. (1) and (2), the ultimate axial strain ε_{cu} is obtained by the following expansion relation equation:

$$\frac{\varepsilon_c}{\varepsilon_{co}} = \left(1.0 + 8.0\frac{\sigma_l}{f'_{co}}\right)\cdot\left[0.970\left(\frac{-\varepsilon_l}{\varepsilon_{co}}\right)^{0.431} + 0.067\left(\frac{-\varepsilon_l}{\varepsilon_{co}}\right)\right] \tag{6}$$

where ε_{co} corresponds to the strain at the peak unconfined concrete stress, which is defined by $\varepsilon_{co} = 2f_{co}'/E_c$, σ_l is the FRP jacket's instantaneous lateral confinement, which is defined by $\sigma_l = 2E_{frp}t_{frp}\varepsilon_h/D$; ε_h is the hoop strain of the FRP with $\varepsilon_h = -\varepsilon_l$. Similarly, the second turning point strain ε_t* is determined by bringing the transition point of the tensile stress–strain relationship of LRS FRP composites into Eq. (6) (0.0083 for PEN FRP and 0.0068 for PET FRP). Notably, for columns wrapped with conventional FRP, only the first linear segment is considered in Eqs. (1) and (2) and $\varepsilon_t^* = \varepsilon_{cu}$. More details of the envelope can be found in Bai et al. [17].

3.2. Unloading and reloading paths

It can be observed from experimental results that the unloading and reloading paths form a loop [8,24]. As shown in Fig. 2, $\varepsilon_{un,env}$ and $\sigma_{un,env}$ are termed as envelope unloading strain and stress, respectively. The unloading path intersects the strain axis at a value referred to as the plastic strain ε_{pl}. ε_{re} and σ_{re} correspond to reloading strain and reloading stress at the beginning of reloading path. A large number of researchers have proposed various formulas to fit the shape variations of unloading and reloading curves for FRP-confined concrete [8,10,11,14,22,36]. Although the empirical equations agree very well with the experimental results, the mathematical expressions are usually too complicated for practical application. In view of this, a linear cyclic rule is proposed in this paper to simulate the stress–strain curve for FRP-confined concrete under cyclic axial compression (see Fig. 2). It is well known from existing studies [8,10] that the unloading and reloading curves are closely related to the plastic strain, envelope unloading strain and stress. The following linear cyclic rule is therefore defined as:

$$\sigma_c = \frac{\sigma_{un,env}}{\varepsilon_{un,env} - \varepsilon_{pl}}(\varepsilon_c - \varepsilon_{pl}) \tag{7}$$

As seen in Fig. 2, the partial unloading and reloading curves up to a predetermined point are denoted by a portion of the complete unloading and reloading paths of the specimen. It is evident from Eq. (7) that the plastic strain is a key parameter for modeling the linear unloading and reloading responses. The next section will focus on the determination of the plastic strain.

3.3. Plastic strains

It is believed that the plastic strain is caused by the collapse of small voids in concrete and the mechanical slippage between coarse aggregate and mortar [42]. Accurate prediction of the plastic strains is usually crucial for the final outcome of a cyclic FRP-confined concrete model. Previous studies have demonstrated a linear relationship exists between plastic strain and envelope unloading strain for FRP-confined concrete [6,8,10-12]. Among these models, the plastic strain equation of the Lam and Teng [8] model has been well accepted for its capacity in producing accurate predictions for the experimental plastic strains of conventional FRP-confined concrete. This equation took into account the strength of

Table 3
Equations for the plastic strain of envelope cycles.

Model	Residual plastic strain ε_{pl}
Lam and Teng [8]	$\varepsilon_{pl} = \begin{cases} 0, & 0 < \varepsilon_{un} \leqslant 0.001 \\ \left[1.4\left(0.87 - 0.004f'_{co}\right) - 0.64\right](\varepsilon_{un} - 0.001), & 0.001 < \varepsilon_{un} < 0.0035 \\ \left(0.87 - 0.004f'_{co}\right)\varepsilon_{un} - 0.0016, & 0.0035 \leqslant \varepsilon_{un} \leqslant \varepsilon_{cu} \end{cases}$
Bai et al. [36]	$\varepsilon_{pl} = \begin{cases} 0, & 0 < \varepsilon_{un} \leqslant 0.001 \\ 0.353\left(\frac{f_{co}}{f_{30}}\right)^{-0.4}(\varepsilon_{un} - 0.001) + 3.36\rho^{-0.178}(\varepsilon_{un} - 0.001)^{1.414} & 0.001 < \varepsilon_{un} \leqslant \varepsilon_t^* \\ -0.342\left(\frac{f_{co}}{f_{30}}\right)^{-0.4}(\varepsilon_{un} - 0.001) + 1.73(\rho^*)^{0.043}(\varepsilon_{un} - 0.001)^{1.217} & \varepsilon_t^* < \varepsilon_{un} \leqslant \varepsilon_{cu} \end{cases}$

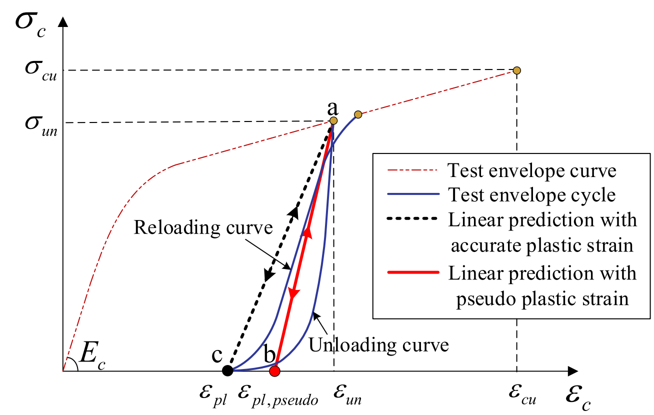

Fig. 4. Comparison of linear prediction with accurate plastic strain and pseudo-plastic strain.

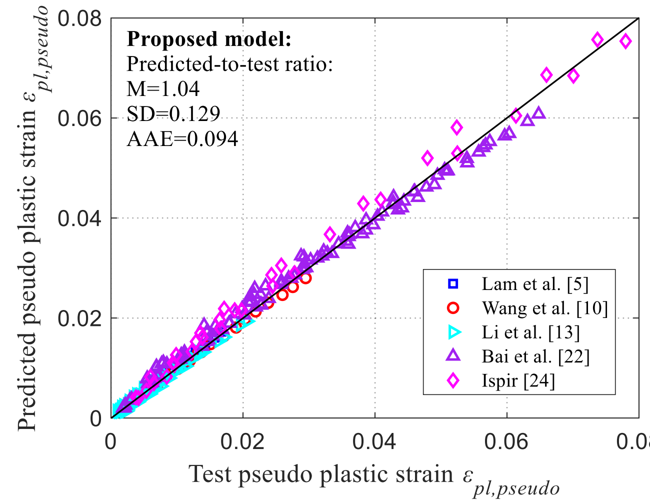

Fig. 6. Performance of proposed pseudo-plastic strain model for envelope cycles.

unconfined concrete and was established based on a linear relationship between the envelope unloading strain and plastic strain. Recently, Bai et al. [36] developed a plastic strain equation for estimating the plastic strain in LRS FRP-confined concrete taking into consideration LRS FRP's two-stage confinement rigidity property. Fig. 3a and b compare the experimental plastic strains from the collected database with the predictions of two plastic strain models provided in Table 3. Three statistical parameters, mean value (M), standard deviation (SD) and average absolute error (AAE), were used to assess the two plastic strain models and their accompanying Eqs. (8), (9), and (10), are expressed respectively as follows:

$$M = \frac{\sum_{i=1}^{n}\left|\frac{theo_i}{exp_i}\right|}{n} \tag{8}$$

$$SD = \sqrt{\frac{\sum_{i=1}^{n}\left[\frac{theo_i}{exp_i} - \left(\frac{theo}{exp}\right)_{aver}\right]^2}{n-1}} \tag{9}$$

$$AAE = \frac{\sum_{i=1}^{n}\left|\frac{exp_i - theo_i}{exp_i}\right|}{n} \tag{10}$$

where n is the quantity of data points, exp_i is the ith experimental value, and $theo_i$ is the ith theoretical value.

As shown in Fig. 3, both models can give reasonable plastic strain predictions for conventional and LRS FRP-wrapped concrete cylinders. Moreover, the Bai et al. [36] model can give more precise expectations in terms of the M, SD and AAE values due to its consideration of the confining stiffness change. However, as mentioned in the introduction section, in order to speed up the calculation efficiency and facilitate easier practical engineering application, the proposed simplified plasticity damage model in this paper adopts a linear cyclic rule to simulate the experimental unloading and reloading curves. The typical test curves in Fig. 4 clearly show that the unloading curve has a softening section when it is close to 0 stress. The degree of nonlinearity in an unloading path increases with the plastic strain, which is particularly obvious for LRS FRP-confined concrete at the later loading stage due to its large rupture strain capacity [22]. Thus, if the accurate plastic strain model like Lam and Teng [8] or Bai et al. [36] is directly applied to the simplified model, the predictive linear cyclic curve (ac) will deviate greatly from the test unloading and reloading curves at a larger plastic strain level (see Fig. 4.

As a result, in order to replicate the overall performance of each cycle with a straight line ("ab" in Fig. 4, a pseudo-plastic strain, $\varepsilon_{pl,pseudo}$, has been proposed in this paper. In total, 344 single experimental unloading and reloading curve results were obtained from the collected database. For a given test cycle, the stiffness of the linear unloading and reloading paths E_{un} was firstly defined as the slope of linear best-fit approximations of all points on this cycle; then, the corresponding intersection point to the strain axis could now be identified as the pseudo-plastic strain (see Fig. 4). According to this concept, a total of 344 pseudo-plastic strains

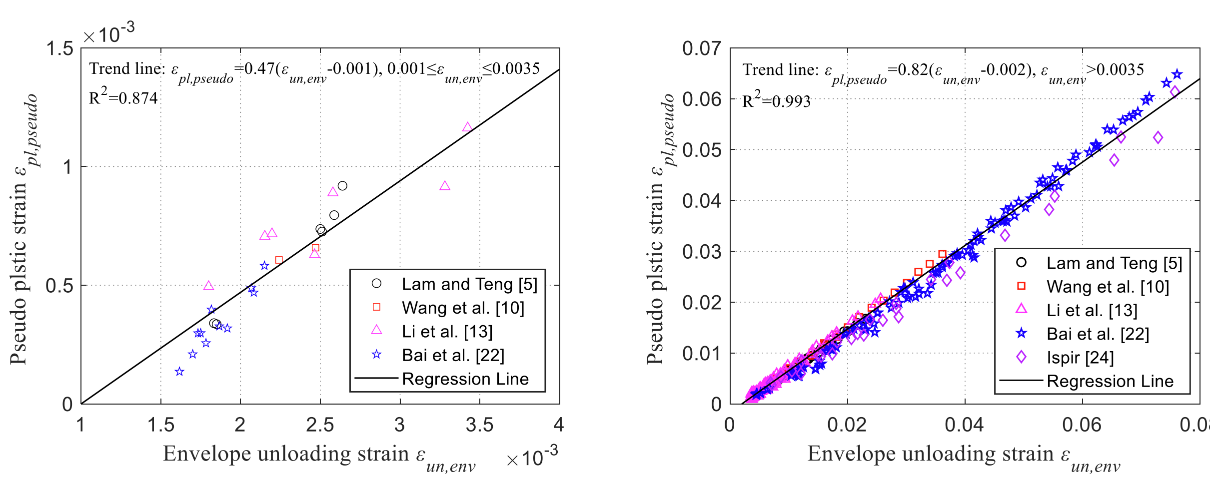

Fig. 5. Relationship between the pseudo-plastic strain and envelope unloading strain.

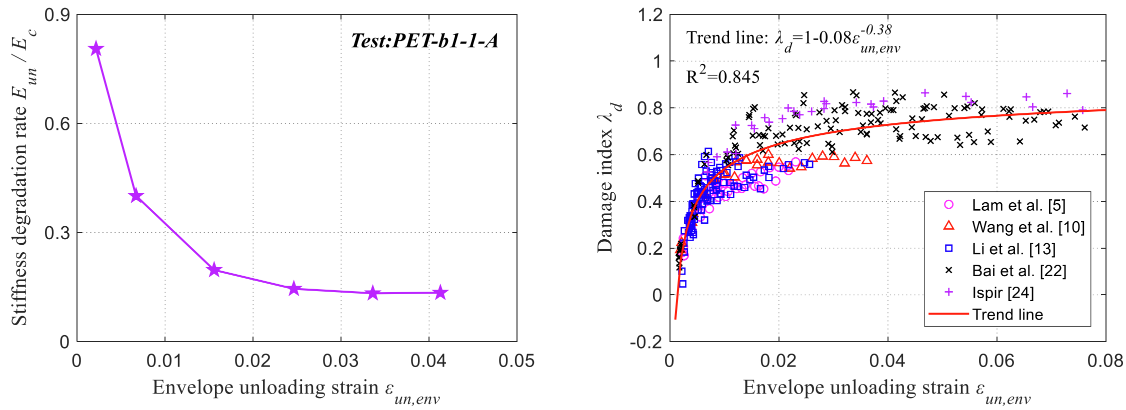

(a) Stiffness degradation process of specimen PET-b1-1-A

(b) Relationship between damage coefficient and envelope unloading strain

Fig. 7. Stiffness degradation of FRP-confined concrete.

can be calculated from the test database, and these results are plotted with the corresponding envelope unloading strains in Fig. 5. This graph demonstrates that the pseudo-plastic strain is linearly associated with the envelope unloading strain of conventional and LRS FRP-confined concrete. Subsequently, by regression analysis between envelope unloading strains and the corresponding pseudo-plastic strains, the following solution was obtained:

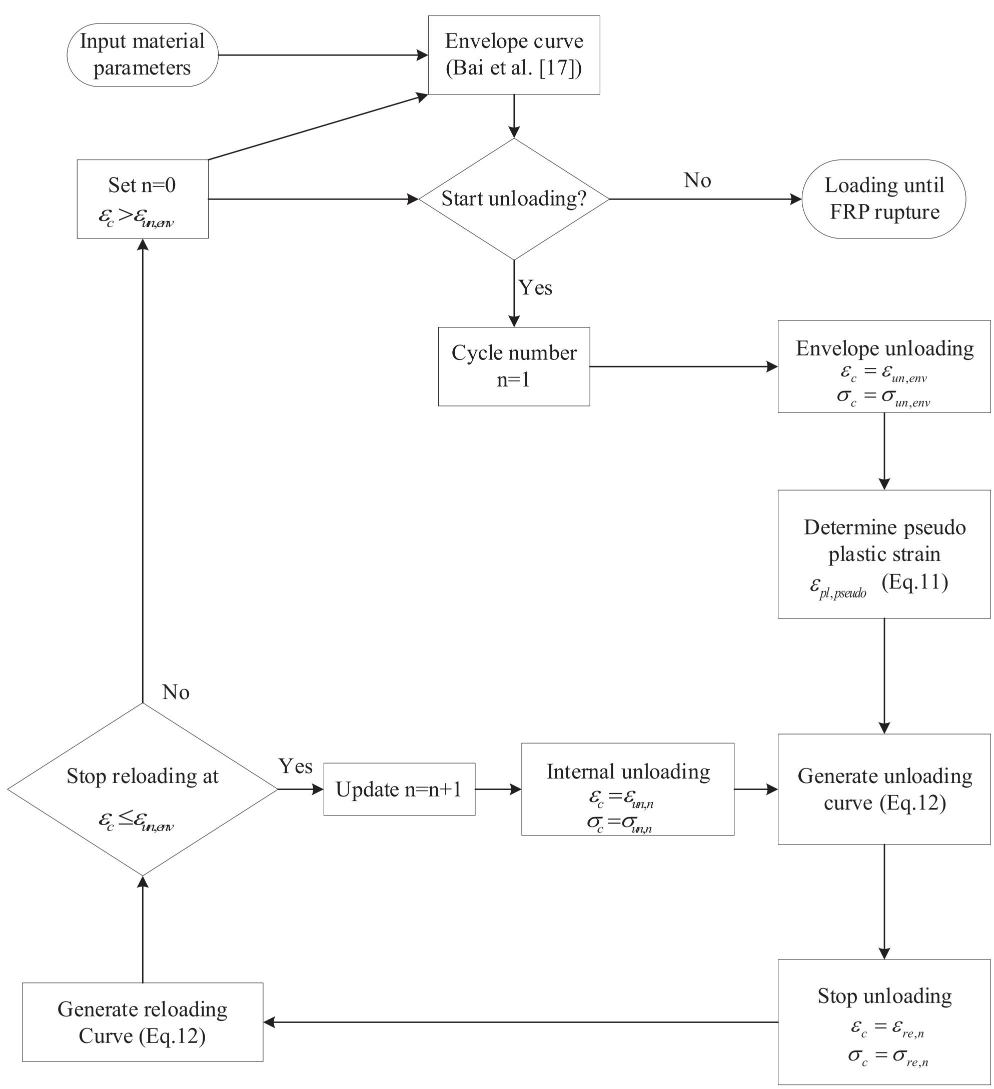

Fig. 8. Flowchart for generation of simplified stress–strain curves under cyclic axial compression.

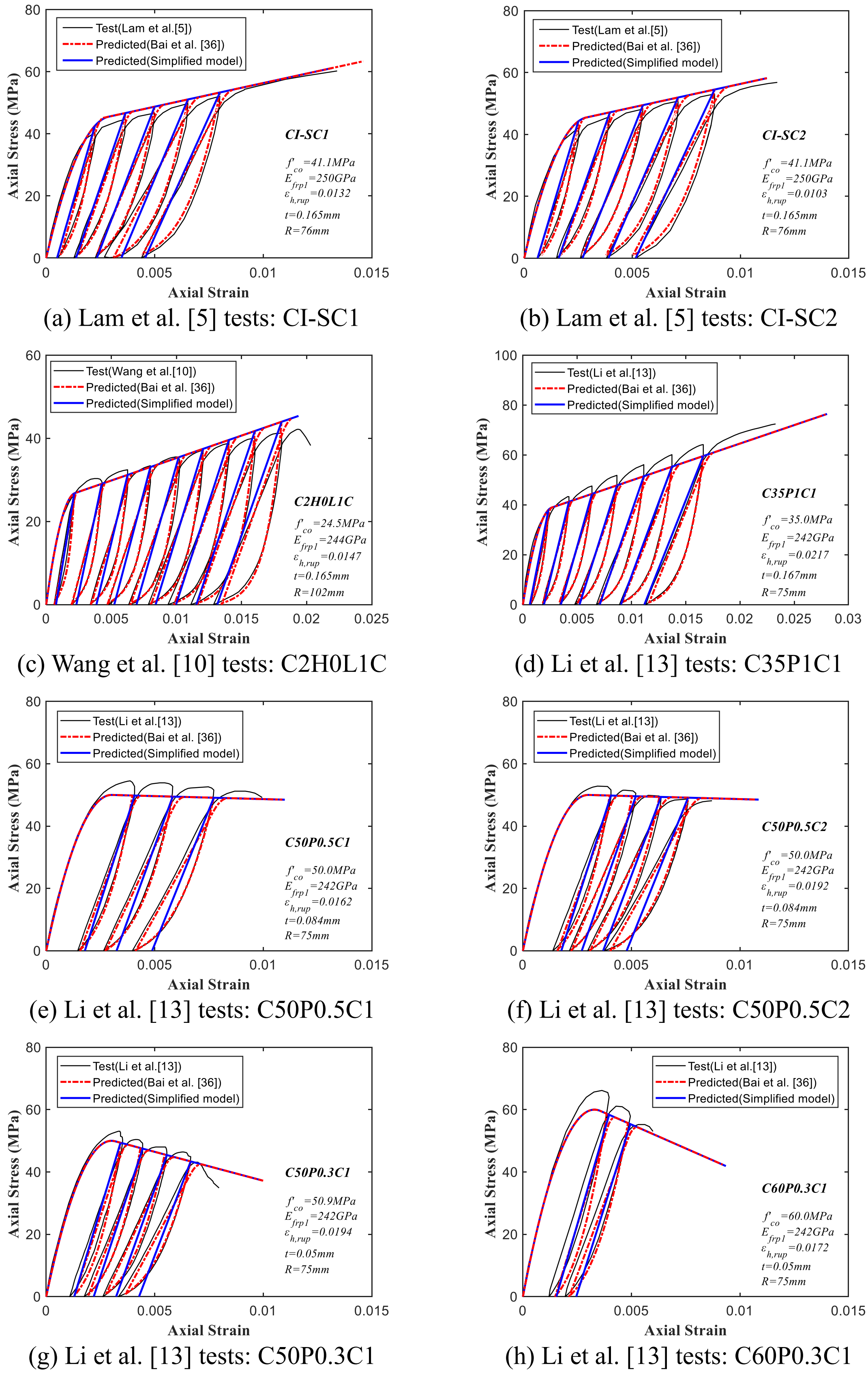

Fig. 9. Performance of simplified model and Bai et al. model [36]: conventional FRP-confined concrete under cyclic axial compression.

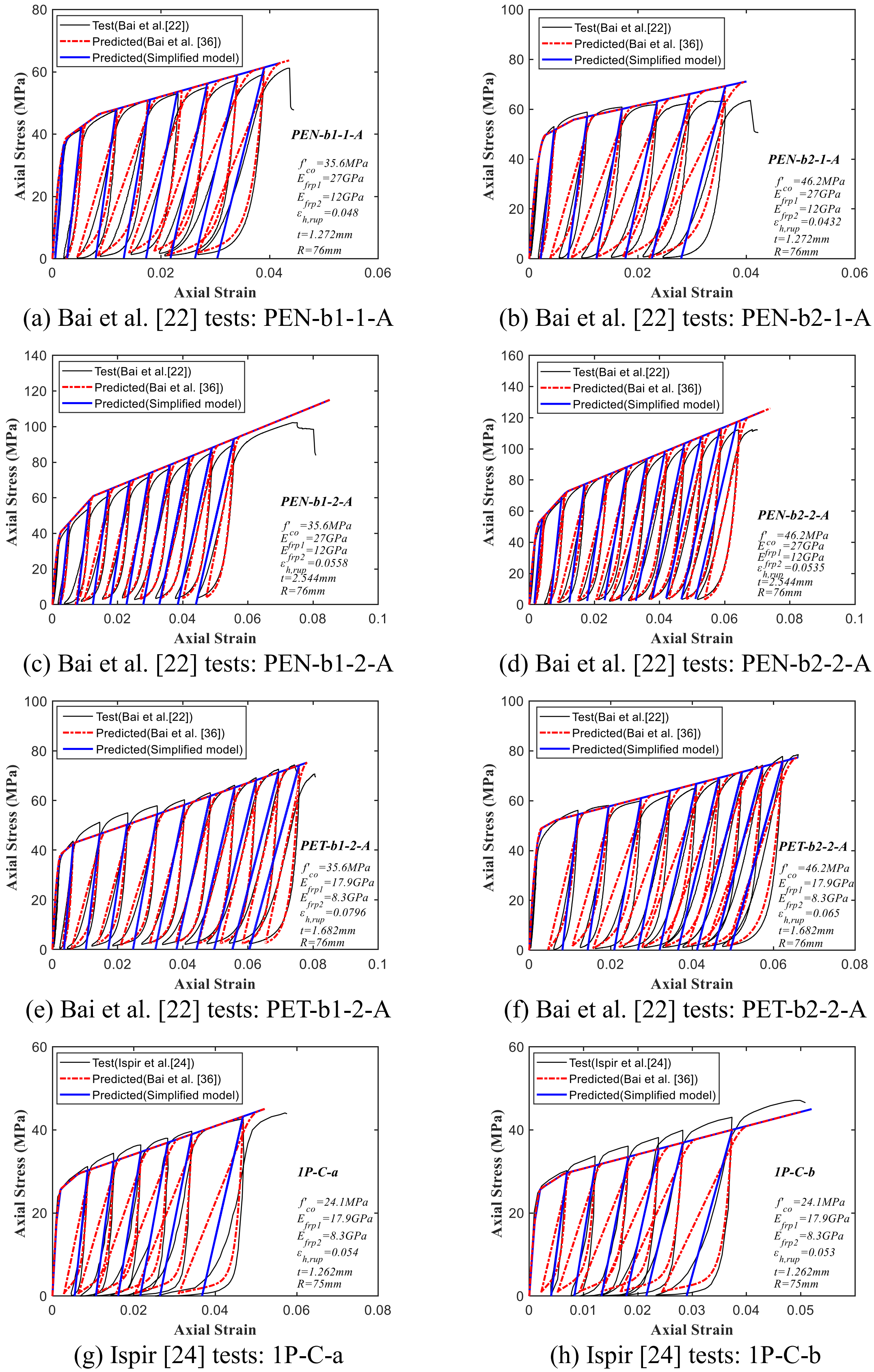

Fig. 10. Performance of simplified model and Bai et al. model [36]: LRS FRP-confined concrete under cyclic axial compression.

Table 4
Key information of selected test columns.

		Dimension		concrete		Longitudinal steel			FRP jacket					Axial load
Reference	Test columns	D (mm)	L (mm)	$f_{co}{}'$ (MPa)	c (mm)	D_s (mm)	n	f_y (MPa)	type	t_j (mm)	E_{frp1} (GPa)	E_{frp2} (GPa)	ε_j	P (kN)
Haroun et al. [3]	CS-R1	610	2438	40.82	19.1	19.1	20	299.3	Carbon	0.671	231.7	–	0.018	635
Saadatmanesh et al. [45]	C-4	305	1801	36.6	6.7	12.7	14	358	NA					445
	C-5	305	1801	36.5	6.7	12.7	14	358	Glass	5	18.6	–	0.029	445
Bai [46]	C-0	238	1250	35.0	16	16	6	450	NA					400
	C-PEN-1	238	1250	35.0	16	16	6	450	PEN	1.272	27	12	0.062	400
	C-PEN-3	238	1250	35.0	16	16	6	450	PEN	3.816	27	12	0.062	400

Note: D, L = diameter and height of test column; $f_{co}{}'$ = concrete cylinder strength; c = cover thickness; D_s, n, f_y = diameter, number, and yield stress of longitudinal steel bars; t_j, E_{frp1}/E_{frp2}, and ε_j = thickness, elastic modulus, and ultimate tensile strain of FRP jacket. P = applied axial load.

$$\varepsilon_{pl,pseudo}\begin{cases} = 0 & 0 < \varepsilon_{un,env} < 0.001 \\ = 0.47\left(\varepsilon_{un,env} - 0.001\right) & 0.001 \leqslant \varepsilon_{un,env} \leqslant 0.0035 \\ = 0.82\left(\varepsilon_{un,env} - 0.002\right) & \varepsilon_{un,env} > 0.0035 \end{cases} \quad (11)$$

In Fig. 6, the proposed pseudo-plastic strain model was evaluated in the same way as adopted in Lam and Teng [8] and Bai et al. [36]. It is easily seen in Fig. 6 that the mean value (M) of the pseudo-plastic strain predicted by the proposed formula is quite close to 1.0, and its SD and AAE values are very small. Thus, the calculations in Eq. (11) are capable of predicting pseudo-plastic strains. Eq. (7) is therefore updated as follows:

$$\sigma_c = \frac{\sigma_{un,env}}{\varepsilon_{un,env} - \varepsilon_{pl,pseudo}}\left(\varepsilon_c - \varepsilon_{pl,pseudo}\right) \quad (12)$$

3.4. Stiffness degradation of FRP-confined concrete

The conventional and LRS FRP-confined concrete showed remarkable deterioration in elastic stiffness due to gradual damage accumulation [5,22]. Substantial research was carried out to predict the damage evolution laws of concrete [8,11,14,36,42-44]. The degradation process of elastic unloading and reloading stiffness (the same in the simplified model), E_{un}, can explicitly reflect the damage evolution of concrete. To eliminate the effects of concrete strength on stiffness degradation, the elastic stiffness ratio (the ratio of elastic unloading/reloading stiffness to the initial elastic modulus of concrete E_{un}/E_c) is introduced here. Fig. 7a shows the typical degradation process of concrete stiffness with the increase of the envelope unloading strain by taking PET-b1-2-a of Bai et al. [22] as an example. It is shown that the elastic stiffness ratio decreases with the increase of the envelope unloading strain, which is caused by the expansion of initial defects with the increased number of loading cycles. The value of the elastic stiffness ratio finally stabilizes to a certain value. In this subsection, the damage variable, λ_d, is defined to describe the damage degree of concrete. When λ_d is equal to 0, it means that the concrete is not damaged, and when λ_d is equal to 1, it means that the concrete has been completely damaged. The damage equation of FRP-confined concrete is expressed as:

$$\lambda_d = 1 - \frac{E_{un}}{E_c} \quad (13)$$

The stiffness of the proposed linear unloading and reloading paths can be then calculated as:

$$E_{un} = \sigma_{un,env}/\left(\varepsilon_{un,env} - \varepsilon_{pl,pseudo}\right) \quad (14)$$

Eqs. (13) and (14) illustrate that the damage degree, λ_d, in FRP-confined concrete is dependent on the envelope unloading strain. Li et al.[42] proposed an exponential formula, $d = 1 - a\varepsilon_{un}{}^{-b}$, to reflect the damage degree of steel fiber-reinforced concrete; a and b are coefficients of the damage evolution law designed to control the speed and shape of the damage process. This method is chosen in this study to depict the damage degree of FRP-confined concrete. Fig. 7b shows that with the increase of the envelope unloading strain, the damage of concrete gradually increases and finally tends to be stable. Through regression analysis, the relationship between the damage coefficient, λ_d, and the envelope unloading strain, $\varepsilon_{un,env}$, is obtained as shown in Eq. (15) with the fitting standard deviation of 0.845.

$$\lambda_d = 1 - 0.08\varepsilon_{un,env}^{-0.38} \quad (15)$$

3.5. Flowchart of proposed simplified model

In this study, the cyclic simplified plasticity damage model for LRS FRP-confined concrete adopted the envelope model from Bai et al. [17] and the linear cyclic rule with a pseudo-plastic strain proposed in this paper. The flowchart for creating the simplified cyclic axial stress–strain curves is summarized in Fig. 8 for easy reference.

3.6. Verification of the proposed simplified model

Figs. 9 and 10 compare the predictions of the simplified model and the experimental results selected from Tables 1 and 2. The comparisons indicate that the proposed simplified model performed well in terms of predicting the peak stresses and strains, as well as the shape of the envelope curve for both hardening and softening types. The model also can accurately predict the position of unloading and reloading routes for both conventional and LRS FRP-confined concrete. Moreover, to further evaluate the performance of the proposed simplified model, the predictions from Bai et al. [36] model were added into the comparisons in Figs. 9 and 10. It was found in Fig. 9a-d that the predictions between the two models had very slight discrepancies from the experimental curves of hardening type for conventional FRP-wrapped specimens due to the relatively small plastic strains. However, for conventional FRP-wrapped specimens with softening type curves in Fig. 9e-h and LRS FRP-wrapped specimens in Fig. 10, it was observed that the deviation of plastic strain predicted by the proposed simplified model increases when the unloading strain becomes large. This deficiency was caused by the linear straight approximation adopted in the proposed model. On the other hand, plastic strains predicted by the Bai et al. [36] model were well matched with the experimental results. Generally, although the proposed simplified model can precisely describe the envelope curve for the cyclic axial compression response of FRP-confined concrete and properly depict the unloading and reloading curves with a straight line, the prediction accuracy of plastic strains is to some extent compromised.

4. Seismic performance of FRP-strengthened circular RC piers

OpenSees [39] is well-suited for modeling the seismic behavior of RC columns due to its efficiency and accuracy. In this section, the proposed simplified model was built in C++ language for inclusion in the material library of the OpenSees platform as a new uniaxial material model. Test results of four FRP-jacketed circular RC columns reported in the open

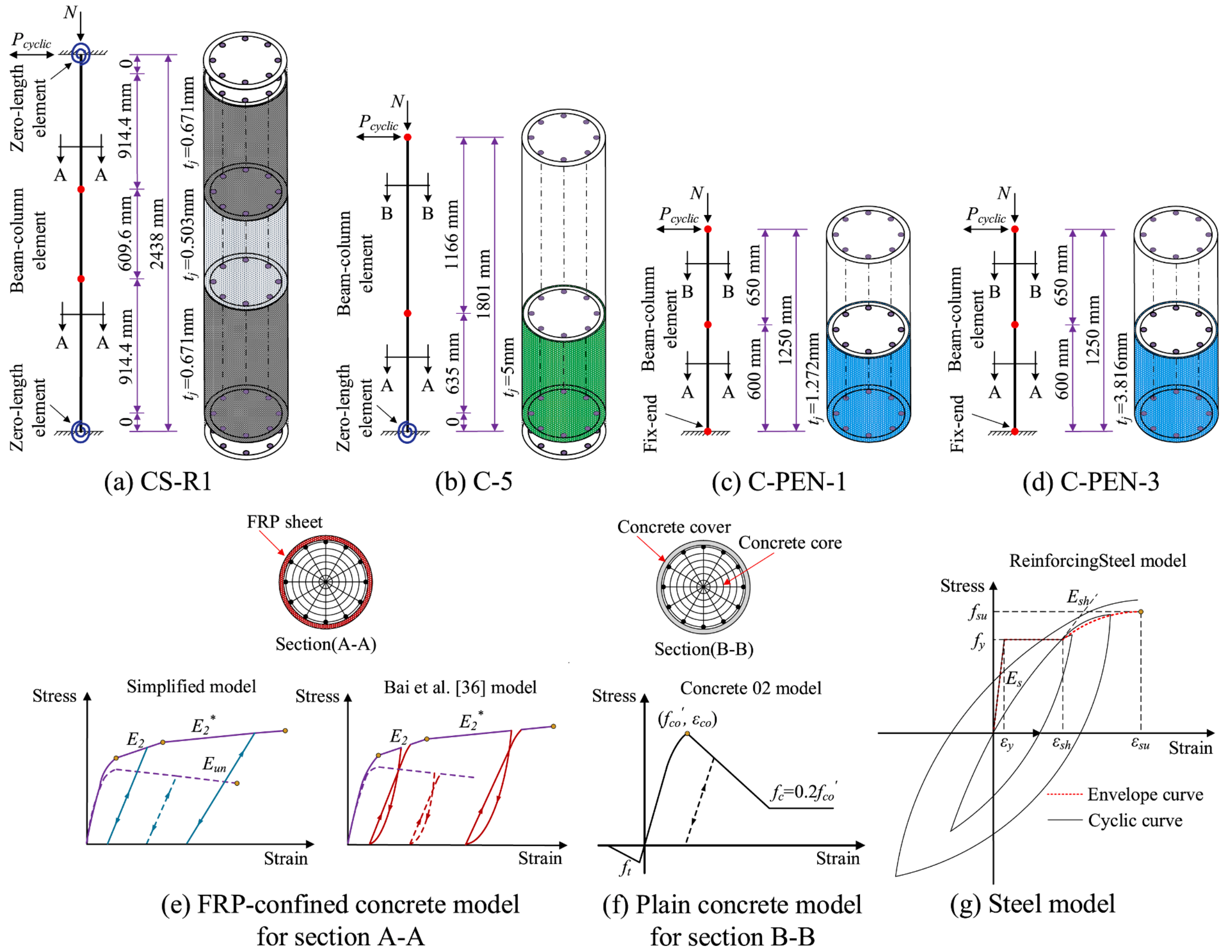

Fig. 11. Modeling of fully and partially wrapped circular columns in OpenSees.

literature [3,45,46], including two conventional FRP-confined and two PEN FRP-confined RC columns, were modeled based on the proposed model. The selected RC columns were subjected to a constant axial load in combination with a lateral cyclic load. Among these columns, specimen CS-R1 was subjected to double-curvature bending, while the other three specimens, C-5, C-PEN-1 and C-PEN-3, were subjected to single-curvature bending. For comparison purposes, their unwrapped counterpart specimens were also simulated except for specimen CS-R1 in Haroun et al. [3], which failed by brittle shear failure. Detailed information of the chosen columns is listed in Table 4. In the simulation, the ultimate rupture strain of the FRP jacket was needed to determine the final state of the FRP-confined concrete. Teng et al. [35] claimed that using the tensile fracture strain of FRP obtained from a flat coupon test in the simulation does not lead to an overestimation of the experimental results. Therefore, in the simulation, the rupture stain of FRP from the flat coupon tensile test was used as the input value for determining the ultimate state of the FRP-confined concrete. This is an acceptable approximation; however, more work is needed to verify the experimental results [35].

4.1. OpenSees numerical modeling details

The simulated height of each column was from the bottom of the column to the position where the lateral load was applied. As shown in Fig. 11a, CS-R1 was a full column wrapped CFRP, which was divided into three segments according to the thickness variation of the FRP in the confined area. For the other three selected specimens, C5, C-PEN-1, and C-PEN-3 in Fig. 11b-d, only the plastic hinge zone area was wrapped with an FRP jacket. These columns were divided into two segments, namely the FRP-confined part and the upper part. All divided segments were simulated in OpenSees using the NonlinearBeamColumn element with four integration points. This type of element is a force-based element and considers geometric nonlinearity and plastic propagation. For the selected columns, the experimental initial stiffness of the specimens showed that some rotations occurred between the ends of specimens, CS-R1 and C5, and the actuators. However, this phenomenon in specimens C-PEN-1 and C-PEN-1 was not significant. Therefore, a zero-length element was employed at the ends of specimen CS-R1 and C5 to represent these additional rotations [26,35], but the ends of specimen C-PEN-1 and C-PEN-1 were fixed, as seen in Fig. 11a-d. The column cross section adopted a fiber section method and was divided into 10 radial and 20 circumferential partitions. This degree of division was shown to provide adequately precise findings in accordance to other comparable discretization methods [1,35].

For the column section encased in an FRP jacket, the concrete material was simulated with the proposed simplified model. In addition, the recently developed design-oriented cyclic model of Bai et al. [36] was implemented in OpenSees in the same way to compare and evaluate the predictions of the simplified model for the hysteretic behavior of FRP-strengthened circular RC columns, as shown in Fig. 11e. The confinement effect supplied by transverse reinforcements was neglected in the FRP-confined zone due to the sparse transverse reinforcement arrangement in the selected specimens. However, in the simulation of the non-FRP region, the confinement provided by transverse reinforcement was considered by dividing the section into the confined concrete core and the unconfined concrete cover using the Concrete02 material model (Fig. 11f). The peak stress and ultimate strain of concrete outside the FRP-confined region were calculated using the concrete model of

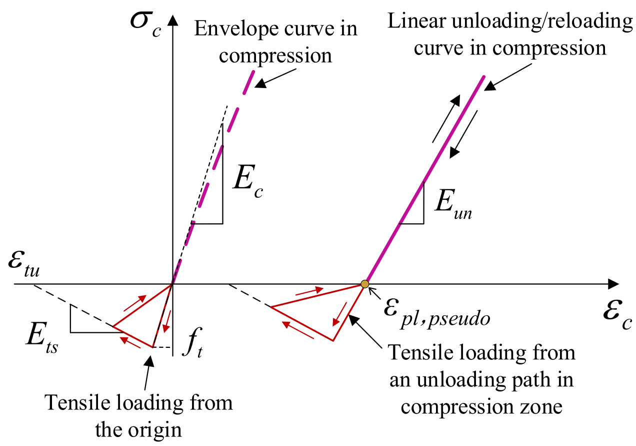

Fig. 12. Cyclic tension stress–strain curve of simplified model.

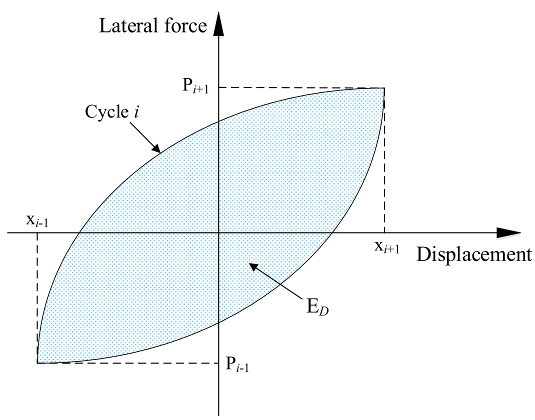

Fig. 13. Calculation model of energy dissipation.

Mander et al. [47]. The stress of all concrete materials after failure was considered to be equal to $0.2f_{co}$'. The longitudinal reinforcements were simulated by "ReinforcingSteel" model, which was proved to be well suited for simulation of the RC column cross-section with its discrete fiber section [48] (Fig. 11g).

The Concrete02 model in OpenSees was proposed by Yassin [49], which is capable of describing concrete's tensile behavior. The tensile stress–strain envelope of the Concrete02 model is composed of a linear rising segment and a linear descending segment. The slope of the rising segment is equal to the initial elastic modulus of concrete E_c and the descending segment is defined as the linear connection between the tensile strength point and the ultimate tensile strain point. The tensile strength equation for concrete is $f_t = 0.632\sqrt{f_{co}'}$, and the ultimate tensile strain is $\varepsilon_{tu} = f_t\,(1/E_{ts} + 1/E_c)$, where E_{ts} is the tensile softening stiffness (equal to $0.05E_c$). In the tensile part of the Concrete02 model, the unloading and reloading paths are also defined as a linear line between the unloading point and the starting point of the tensile load, as shown in Fig. 12 the tensile point located at the origin.

Since the cyclic tension mode of the Concrete02 model ignores the impact of compressive degradation on the tensile stiffness of concrete, Teng et al. [35] modified this model by assuming that the tensile stiffness of concrete equals the compressive stiffness $E_{un,0}$, which is taken as minimum of $0.5f_{co}'/\varepsilon_{un}$ and $\sigma_{un}/(\varepsilon_{un} - \varepsilon_{pl})$. A special condition is that the tension at the origin of the concrete has a tensile stiffness equal to E_c. This refinement guarantees that the stress–strain curve's slope is consistent from the compression region to the tension region. For these reasons, this paper used the Teng et al. [35] method to depict the concrete in tension. The tensile modulus of concrete in the present study is equal to the linear unloading and reloading stiffness defined by Eq. (14). The definition of the simplified model's tensile zone is illustrated in Fig. 12. All numerical simulations were performed using the principles and factors specified here, unless otherwise specified.

4.2. Numerical results for seismic analysis

In the hysteretic behavior analysis of the specimens, the lateral displacements identical to those logged during the experiment were used for simulation. The analysis stops once the axial strain of concrete reaches the ultimate state described in the simplified model or the lateral displacement of the specimen reaches the experimentally recorded value. The energy dissipation calculation model of the test column is demonstrated in Fig. 13. The energy dissipation value E_D of the column is the area included in the hysteretic curve of each cycle. P_{i+1} and $P_{i\text{-}1}$ represent the maximum and minimum load values of cycle i, respectively. x_{i+1} and $x_{i\text{-}1}$ represent the maximum and minimum displacement values of the cycle i, respectively.

Fig. 14 shows the comparison of the predicted load–displacement curves of the unwrapped control specimens with the test results. In general, numerical simulations based on the OpenSees gave close predictions for the load–displacement curves. It should be mentioned that for specimen C-4 in Saadatmanesh et al. [45], the simulation terminated in advance due to convergence reasons before the arrival of the ultimate test displacement, which was caused by concrete crushing and severe buckling of longitudinal reinforcements. Figs. 15 and 16 compare the predictions of the simplified model with the Bai et al. [36] model. The

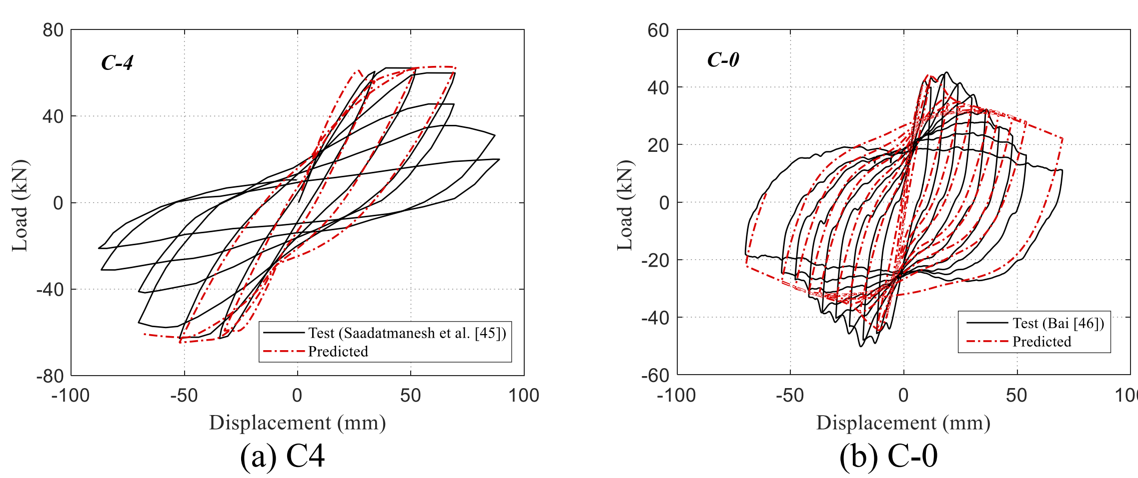

Fig. 14. Load-displacement curves of unwrapped control specimens.